

**Non peer-reviewed preprint submitted to Environmental Research Letters**

## **Controls on coastal saline groundwater across North America**

Daniel V. Kretschmer<sup>1\*</sup>, Holly A. Michael<sup>2</sup>, Nils Moosdorf<sup>3</sup>, Gualbert H. P. Oude Essink<sup>4</sup>, Marc F. P. Bierkens<sup>5</sup>, Thorsten Wagener<sup>1</sup>, Robert Reinecke<sup>6</sup>

<sup>1</sup>Institute of Environmental Science and Geography, University of Potsdam, Potsdam, Germany

<sup>2</sup>Department of Earth Sciences, University of Delaware, Newark, Delaware, USA

<sup>3</sup>Leibniz Centre for Tropical Marine Research (ZMT), Bremen, Germany

<sup>4</sup>Unit Subsurface and Groundwater Systems, Deltares, Utrecht, Netherlands

<sup>5</sup>Department of Physical Geography, Utrecht University, Utrecht, Netherlands

<sup>6</sup>Institute of Geography, Johannes Gutenberg-University Mainz, Mainz, Germany

\*Correspondence: Daniel V. Kretschmer ([daniel.kretschmer@uni-potsdam.de](mailto:daniel.kretschmer@uni-potsdam.de))

1 **Controls on coastal saline groundwater across North America**

2 Daniel V. Kretschmer

3 Institute of Environmental Science and Geography, University of Potsdam, Potsdam, Germany

4

5 Holly A. Michael

6 Department of Earth Sciences, University of Delaware, Newark, Delaware, USA

7

8 Nils Moosdorf

9 Leibniz Centre for Tropical Marine Research (ZMT), Bremen, Germany

10

11 Gualbert H. P. Oude Essink

12 Unit Subsurface and Groundwater Systems, Deltares, Utrecht, Netherlands

13

14 Marc F. P. Bierkens

15 Department of Physical Geography, Utrecht University, Utrecht, Netherlands

16

17 Thorsten Wagener

18 Institute of Environmental Science and Geography, University of Potsdam, Potsdam, Germany

19

20 Robert Reinecke

21 Institute of Geography, Johannes Gutenberg-University Mainz, Mainz, Germany

22

23 Corresponding author: Daniel V. Kretschmer (dkretsch@uni-mainz.de)

24 **Abstract**

25 Groundwater is crucial to sustaining coastal freshwater needs. About 32 million people in the  
26 coastal USA rely on groundwater as their primary water source. With rapidly growing coastal  
27 communities and increasing demands for fresh groundwater, understanding controls of continental-  
28 scale coastal groundwater salinity is critical. To investigate what hydrogeological factors (e.g.,  
29 topography, hydraulic conductivity) control coastal saline groundwater at continental scales, we  
30 have simulated variable-density groundwater flow across North America with the newly developed  
31 Global Gradient-based Groundwater Model with variable Densities (G<sup>3</sup>M-D). The simulation

32 results suggest that under a steady climate and pre-development conditions (i.e., steady 30-year  
33 mean groundwater recharge, no withdrawals nor sea level rise) saline groundwater is present in  
34 18.6% of North America's coastal zone, defined as up to 100 km inland and up to 100 m above  
35 mean sea level. We find that the coastal zone is particularly vulnerable to containing saline  
36 groundwater at low hydraulic gradients ( $<10^{-4}$ ) and large hydraulic conductivities ( $>10^{-2}$  m day<sup>-1</sup>).  
37 To analyze model parameter sensitivities, i.e., which parameters control the resulting distribution  
38 of saline groundwater, we utilize the inherent spatial model variability. We find that hydraulic  
39 gradient, topographic gradient, hydraulic conductivity, and aquifer depth are important controls in  
40 different places. However, no factor controls coastal groundwater salinization alone, suggesting  
41 that parameter interactions are important. Using G<sup>3</sup>M-D based on G<sup>3</sup>M, a model that previous work  
42 found to be strongly controlled by topography, we find no controlling influence of recharge  
43 variability on the saline groundwater distribution in North America. Despite a likely overestimation  
44 of saline interface movement, the model required 492 000 years to reach a near-steady state,  
45 indicating that the saline groundwater distribution in North America has likely been evolving since  
46 before the end of the last ice age, approximately 20 000 years ago.

## 47 **1. Introduction**

48 Coastal groundwater is vital to sustaining coastal freshwater consumption and agricultural activities  
49 in the US (Barlow and Reichard, 2010) and other countries worldwide (Custodio, 2010; Shi and  
50 Jiao, 2014; Manivannan and Elango, 2019). About half of all coastal counties (143 of 297) in the  
51 US, home to 32 million people, rely on groundwater as their main water supply (Dieter et al., 2018).  
52 Between 1960 and 2008, the population in coastal counties in the US grew by over 80%, 20% more  
53 than non-coastline counties (Wilson and Fischetti, 2010). Over a similar period, from 1950 to 2015,  
54 the growing demand for freshwater led to a doubling of groundwater withdrawal in the US (Dieter  
55 et al., 2018), causing hydraulic gradients at the coast to reduce and even turn landward (Jasechko  
56 et al., 2020).

57 Where hydraulic gradients at the coast decline (e.g., due to a drop in the groundwater table or  
58 relative to sea level rise), saline ocean water may intrude into the groundwater system and salinize  
59 freshwater aquifers. In addition to growing water demand, storm surges and sea-level changes may  
60 exacerbate seawater intrusion (Post et al., 2018). Seawater intrusion has already affected coastal  
61 groundwater across North America (Barlow and Reichard, 2010). Worldwide, nearly a third of all  
62 coastal metropolises are threatened by seawater intrusion (Cao et al., 2021). However, our

63 understanding of the rapidly changing coastal groundwater lacks predictive capabilities  
64 (Richardson et al., 2024), which is why we need to better understand dominant controls of coastal  
65 saline groundwater and how these vary along coastlines.

66 Several continental and global studies have addressed the issue of seawater intrusion. In a study of  
67 the US coast, Ferguson & Gleeson (2012) show that groundwater withdrawal in coastal regions is  
68 a greater control on horizontal seawater intrusion than sea level rise or changes in groundwater  
69 recharge. Based on estimated submarine groundwater discharge and groundwater withdrawals, 9%  
70 of the contiguous United States coastline are vulnerable to seawater intrusion (Sawyer et al., 2016).  
71 Resilience against seawater intrusion driven by sea level rise is higher when groundwater levels  
72 within aquifers can shift upwards, balancing the gradient change induced by sea level rise (Michael  
73 et al., 2013). In other words, aquifers are more resilient where the topographic gradient to the coast  
74 remains larger than the hydraulic gradient to the coast as sea-level rise progresses. Similarly,  
75 groundwater simulations along the coast of California show that coastal topography controls  
76 seawater intrusion and overland flooding due to sea-level rise (Befus et al., 2020). Recently  
77 published results from groundwater models in 1 200 coastal regions around the world suggest that  
78 coastal fresh groundwater volumes will decrease by about 5% until 2100 due to sea-level rise  
79 (Zamrsky et al., 2024). They confirmed previous findings showing higher resilience against  
80 seawater intrusion in regions with higher topographic gradients, often aligning with steeper  
81 hydraulic groundwater gradients.

82 However, previous simulations of coastal groundwater share a major limitation: their model extent  
83 is limited landward, thus requiring assumptions about the landward boundary condition (Michael  
84 et al., 2013; Zamrsky et al., 2024), which can strongly impact the results of seawater intrusion  
85 simulations (Werner and Simmons, 2009; Ketabchi et al., 2016). Michael et al. (2013) simulated a  
86 theoretical aquifer to analyze the effect of changing groundwater recharge, hydraulic conductivity,  
87 and anisotropy on the saltwater distribution in the aquifer. However, since the changes were applied  
88 one at a time, their combined effects were not simulated. Further, the only global assessment of  
89 seawater intrusion (Zamrsky et al., 2024) was limited to a quarter of the global coastline with  
90 permeable unconsolidated sedimentary formations. Hence, wide parameter ranges and  
91 combinations remain unexplored. Table S1 shows a comparison of continental and global coastal  
92 groundwater models.

93 Here, we use a Darcy approach (Reinecke et al., 2019b) to simulate groundwater flow of the entire  
94 North American continent under a steady climate (e.g., steady groundwater recharge) and natural,  
95 pre-pumping conditions (i.e., without withdrawals). The density zones are simulated with a SWI2-  
96 like variable density routine (Bakker et al., 2013). Like the problem described by Henry (1964),  
97 the entire groundwater system is fresh in its initial state, ensuring that the ocean is the only source  
98 of saltwater (which is a simplification as saline groundwater can have multiple other sources). As  
99 the over 450 000 model cells were parameterized individually, the model incorporates all  
100 combinations of input parameters existing at the simulated resolution of 5 arcminutes (roughly 9.2  
101 km at the Equator). This allows us to assess which of the impact factors, topographic gradient (dT),  
102 hydraulic gradient (dH), hydraulic conductivity (K), aquifer depth ( $D_{\text{aqu}}$ ), and groundwater  
103 recharge (GWR) control the simulated distribution of saline groundwater.

## 104 2. Methods

### 105 2.1 The global gradient-based groundwater model

106 The global gradient-based groundwater model, G<sup>3</sup>M (Reinecke et al. 2019a; Reinecke et al.,  
107 2019b), was inspired by concepts of MODFLOW-2005 (Harbaugh et al., 2005) and built to be  
108 coupled with global hydrological models. To facilitate the assessment of groundwater at the global  
109 scale, hydraulic gradients between grid cells drive the flow between the cells. The three-  
110 dimensional flow of groundwater is described by a partial differential equation (Harbaugh et al.,  
111 2005):

$$112 \quad \frac{\partial}{\partial x} \left( K_{xx} \frac{\partial h}{\partial x} \right) + \frac{\partial}{\partial y} \left( K_{yy} \frac{\partial h}{\partial y} \right) + \frac{\partial}{\partial z} \left( K_{zz} \frac{\partial h}{\partial z} \right) + W = S_s \frac{\partial h}{\partial t}$$

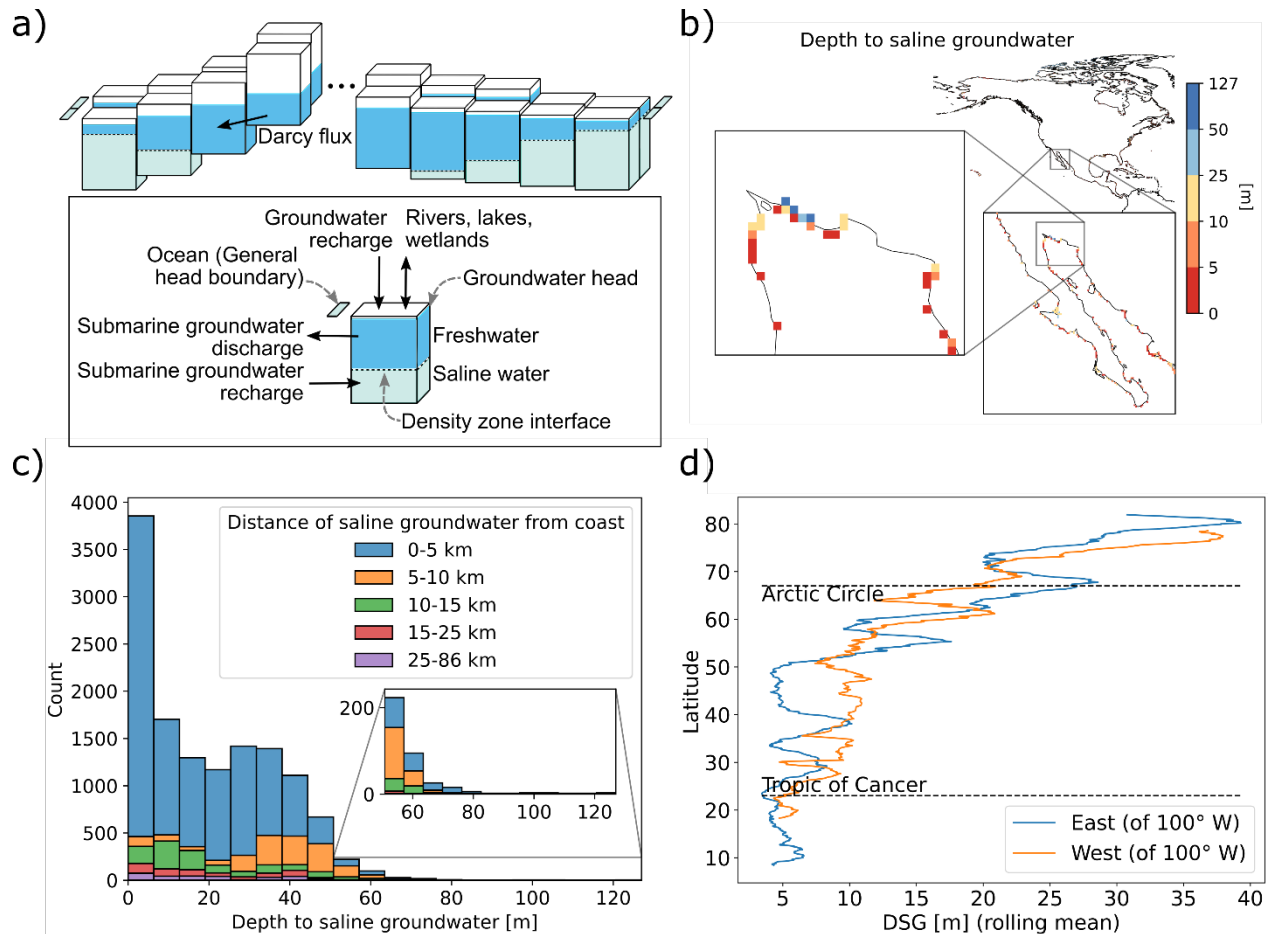
113 where  $K_{xx}$ ,  $K_{yy}$ , and  $K_{zz}$  [ $L^2T^{-1}$ ] are the hydraulic conductivity along the x, y, and z axes between  
114 the cells with sizes  $\Delta x$ ,  $\Delta y$ , and  $\Delta z$  [L];  $S_s$  [ $L^{-1}$ ] is the specific storage;  $h$  [L] is the hydraulic head.  
115  $W$  [ $T^{-1}$ ] incorporates the flows into and out of each cell, such as groundwater recharge, surface  
116 water bodies (i.e., rivers, lakes, and wetlands), or the ocean. Just like the flows between the cells,  
117 the flow from a cell to a river, lake, wetland, or ocean depends on the respective heads. Thus, each  
118 cell can receive/give water from/to neighboring cells and additionally from/to rivers, lakes,  
119 wetlands, and the ocean. In a coupled state these surface water bodies are updated by the  
120 hydrological model. In this study surface water heads are kept at their initial elevation (30<sup>th</sup>  
121 percentile of a 30 arcsecond digital elevation model; Reinecke et al., 2019b).

## 122 **2.2 The added variable density routine**

123 Freshwater has a lower density than water containing salt. In the newly developed Global Gradient-  
124 based Groundwater Model with variable Densities (G<sup>3</sup>M-D), sharp interfaces lie between density  
125 zones representing salinity levels. The height of these interfaces is simulated similarly to the  
126 Saltwater Intrusion package (SWI2) developed for MODFLOW (Bakker et al., 2013). A SWI2-like  
127 routine was implemented due to its wide range of applications and low simulation cost, which are  
128 essential in developing large-scale models. Compared to G<sup>3</sup>M, which simulates groundwater heads,  
129 G<sup>3</sup>M-D has an additional density interface routine. The groundwater head routine accounts for the  
130 density zone volumes in each cell before solving the variable density equations in the separate  
131 density interface routine. Hence, the mass balance equation (used with constant density) is replaced  
132 by a volume balance equation when simulating variable densities (Text S1 and Bakker et al., 2013).  
133 As density interfaces may need many time steps to develop, multiple shorter variable density time  
134 steps can be simulated per groundwater flow step to reduce simulation time.

### 135 **2.2.1 Density zones and density interfaces**

136 In G<sup>3</sup>M-D, like in SWI2, density zones in each cell are stacked vertically (see Fig 1 a)). The model  
137 calculates the height of horizontal sharp density interfaces, representing the limits of density zones.  
138 Each zone is constant in density (i.e., this corresponds to the discontinuous option in SWI2). In a  
139 setup with one density interface between the two density zones of fresh water and seawater (used  
140 in this study), the density interface represents the approximate location of 50 percent seawater in  
141 the aquifer, neglecting the effects of dispersion and diffusion. In other words, density interface  
142 heights change when the proportions of density zones within a cell change, without simulating a  
143 mixing of density zones. Another limitation is that density can only be inverted between model  
144 layers (i.e., aquifers) but not within the same model layer. While inputs of saline water (i.e., inflow  
145 from a neighboring cell) may cause a density interface to rise, freshwater inputs (i.e., from  
146 groundwater recharge, rivers, or neighboring cells) may induce groundwater flow out of the cell,  
147 potentially lowering the interface height. At each density time step, new interface heights are  
148 computed iteratively for all cells with saline water, followed by interface adjustments. These  
149 adjustments allow the horizontal movement of saline water from a cell with saline water to an  
150 entirely fresh neighboring cell (e.g., when the slope between an interface height and the  
151 neighboring cell bottom is above a threshold). For equations and subroutines of the density routine,  
152 please refer to Text S1 and Bakker et al. (2013).



153  
 154 **Figure 1** – Panel showing a) the concept of the variable density groundwater model (G<sup>3</sup>M-D), b)  
 155 simulated depth to saline groundwater (DSG) at Baja California (for the entire map of North  
 156 America, see Figure S1), c) a histogram of simulated depths to saline groundwater, and d) the  
 157 moving average of DSG on the east and west coast of North America by latitude (separation at  
 158 100° W). The model cell size is 5 arcminutes (~ 9.2 km at the equator).

### 159 2.2.2 Testing the implementation

160 The newly implemented variable density routine was tested using Examples 1 to 3 from the SWI2  
 161 documentation (Bakker et al., 2013). Each example tests different parts of our implementation (see  
 162 Fig S2). Our results in Example 1 show that G<sup>3</sup>M-D can accurately simulate the height change of  
 163 one density interface in an aquifer with an inflow of saline water. Example 2 shows that more than  
 164 one interface can be simulated correctly, simulating two interfaces rotating around the brackish  
 165 zone they enclose. Including three different aquifer layers with changing hydraulic conductivities,  
 166 Example 3 demonstrates that the movement of a density interface between layers is also accurate.

## 167 **2.3 The variable-density groundwater model of North America**

### 168 **2.3.1 Model setup**

169 Several global datasets are used in the G<sup>3</sup>M-D model setup of the North American continent,  
170 including the entire inland. Elevation and surface water bodies (i.e., rivers, lakes, and wetlands) are  
171 parameterized as in Reinecke et al. (2019b). GLHYMPS 2.0 (Huscroft et al., 2018) provided  
172 hydraulic conductivity (mean of model cells: 8.57 m day<sup>-1</sup>) and effective porosity (mean of model  
173 cells: 0.047). Cells with an effective porosity of 0 (56% of the model cells, 20.4% at the coastline)  
174 are excluded from the variable density routine, meaning they cannot hold saline water. The model  
175 does not represent conduits (e.g., in karstic or volcanic aquifers). The groundwater recharge input  
176 was calculated as the 1987-2016 mean from a WaterGAP (Müller Schmied et al., 2020) simulation  
177 using WFDEI (Weedon et al., 2014) as meteorological forcing (mean of model cells: 0.187 mm  
178 day<sup>-1</sup>). The thickness of the single aquifer layer was defined using depth to bedrock data (mean of  
179 model cells: 24.26 m) by Shangguan et al. (2017). This entails that no aquitards or deep confined  
180 aquifers are represented in the model. The input data for elevation, groundwater recharge, effective  
181 porosity, hydraulic conductivity, and aquifer thickness are displayed in Figure S3.

182 A general head boundary (GHB) (Harbaugh, 2005) represents the ocean at all coastline cells and is  
183 set to a constant elevation of 0 m. The coastal shoreline permeability was retrieved from the global  
184 coastal permeability dataset (CoPerm) (Moosdorf et al., 2024) and used to parameterize the GHB  
185 conductance. No groundwater pumping was included in the simulation to assess the coastal saline  
186 groundwater under naturalized conditions. The assumption that the ocean is the only source of  
187 saltwater entails that existing saline groundwater deposits in large parts of North America are  
188 omitted (Feth, 1965; Reilly et al., 2008). Assuming a constant groundwater temperature of 12°C  
189 for the entire North American continent, freshwater (salinity: 0 parts per thousand) was assigned  
190 the density of 999.5 kg/m<sup>3</sup>, and ocean water (salinity: 35 parts per thousand) was assigned the  
191 density of 1 026.6 kg/m<sup>3</sup>. A comparison to other continental or global studies on coastal saline  
192 groundwater is shown in Table S1.

### 193 **2.3.2 Finding stable interface positions**

194 At the start of the simulation, all groundwater in the system was fresh. Over time, saline ocean  
195 water intruded the simulated system through the general head boundary. Since groundwater density  
196 develops significantly slower than the groundwater head, the model was run under pseudo-steady



197 state conditions (Bakker et al., 2013), i.e., with steady sea level, coastline, and recharge, while  
 198 computing changes in density interface heights. Further, one thousand annual density time steps  
 199 were simulated for each groundwater flow time step of thousand years. The simulation was run  
 200 until the interface heights were stable, i.e., the following conditions were satisfied: in two  
 201 consecutive time steps of thousand years the interface height change (a) in 95% of the cells with  
 202 saline water is below 0.05 m and (b) in 99% of the cells with saline water was below 0.1 m. This  
 203 was the case after 492 time steps (i.e., 492 000 years).

204 **2.4 Utilizing spatial variability of inputs and outputs to understand process controls**

205 The groundwater model of North America simulates heads and interface heights in 452 736 cells,  
 206 of which 18 808 are coastline cells (i.e., cells with at least one side facing the ocean). We use the  
 207 intrinsic spatial variability of inputs and outputs in our evaluation to analyze the factors that control  
 208 coastal saline groundwater (similar to Gnann et al., 2023). We consider three aquifer properties:  
 209 aquifer depth, hydraulic conductivity, and topographic gradient, as well as two hydrologic  
 210 characteristics: groundwater recharge and the hydraulic gradient (resulting from the groundwater  
 211 head routine).

212 For all cells containing saline groundwater at the stable state, we evaluate three different aspects of  
 213 coastal saline groundwater: Saline Groundwater Fraction (SGF), Thickness of Fresh Groundwater  
 214 column (TFG), and Distance of saline groundwater from Coast (DC) (Table 1). We separately  
 215 assess factor value distributions in cells with moderate and pronounced (1) saline groundwater  
 216 fraction, (2) thickness of fresh groundwater column, and (3) distance of saline groundwater from  
 217 the coast to assess which factors control the severity of saltwater occurrence in coastal groundwater  
 218 (see Table 1). We repeated this evaluation with increased and decreased thresholds to assess the  
 219 sensitivities of the thresholds separating into moderate and pronounced aspects of coastal saline  
 220 groundwater.

221 **Table 1** – Aspects of coastal saline groundwater with their respective abbreviations and  
 222 explanations.

<b>Aspect of coastal saline groundwater</b>	<b>Abbreviation</b>	<b>Calculated as</b>	<b>Aspect pronounced if</b>
Saline Groundwater Fraction	SGF	Share of saline water in the groundwater column	SGF > 0.5

Thickness of Fresh Groundwater column	TFG	Groundwater head – Interface height	TFG < 5 m
Distance of saline groundwater from coast	DC	Cell distance from the coastline in km	DC > 10 km

223

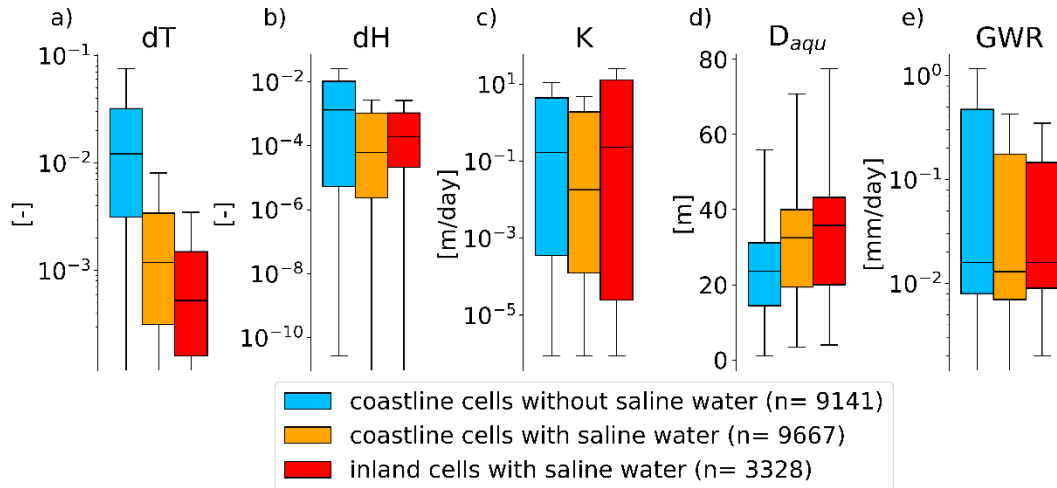
224

### 225 3. Results

226 In the final (stable) state of the salinity interfaces, 12 995 (2.9%) of the 452 736 simulated cells  
227 contained saline groundwater (9 667 of which are coastline cells). The simulated state does not  
228 necessarily represent the current real-world situation. It evolved from an initial entirely fresh  
229 groundwater system and shows the potential spatial distribution of saline groundwater for steady  
230 groundwater recharge and sea level without groundwater pumping or historical marine brine  
231 deposits. The simulated depth to saline groundwater (DSG) in most cells (86%) containing saline  
232 water is less than 40 m (Fig 1 c)), with large regions of shallow saline groundwater in Alaska (US),  
233 Nunavut (Canada), and Oaxaca (Mexico) (Fig 1 b), Fig S3). In both the east and west of North  
234 America, depth to saline groundwater (DSG) reduces from about 50 m in the north to roughly 10  
235 m in the south (Fig 1 d), reflecting the aquifer thickness distribution (Fig S3). In the following, we  
236 examine the sensitivity to the possible impacting factors, i.e., topographic gradient (dT), hydraulic  
237 gradient (dH), hydraulic conductivity (K), aquifer depth ( $D_{\text{aqu}}$ ), and groundwater recharge (GWR)  
238 to find the dominant controls in coastal groundwater salinity on the continental scale.

#### 239 3.1 Topographic gradient and aquifer depth control incursion at the continental coastline

240 Roughly half (i.e., 9 667 of 18 808) of the North American coastline cells (i.e., cells with at least  
241 one side facing the ocean) contain saline water in the stable state, while the other half (9 141) stays  
242 entirely fresh. Figure 2 shows the factor distributions of (1) coastline cells without saline water  
243 (blue), (2) coastline cells with saline water (orange), and (3) inland cells with saline water (red).  
244 Fresh inland cells are omitted in Figure 2. The median topographic gradient (dT) in coastline cells  
245 without saline water (just over 0.02) is one order of magnitude larger than in coastline cells with  
246 saline water (just over 0.002) (Fig 2 a)), mainly because saline water can only enter a model cell if  
247 the sea level is above the aquifer bottom (applies to 66% of coastline cells). The median hydraulic  
248 gradient (dH) in coastline cells without saline water (roughly  $10^{-3}$ ) is one order of magnitude larger  
249 than in cells with saline groundwater at the coastline and inland (Fig 2 b)). Besides topographic  
250 gradient (dT), hydraulic conductivity (K) seems to control the distribution of saline water inland,  
251 since hydraulic conductivity is much higher in inland cells containing saline water (Fig 2 c)).  
252 Further, cells with saline water tend to have a larger aquifer depth (Fig 2 d)) and groundwater  
253 recharge (GWR) can be much higher in fresh coastline cells than in cells with saline groundwater  
254 (Fig 2 e)).

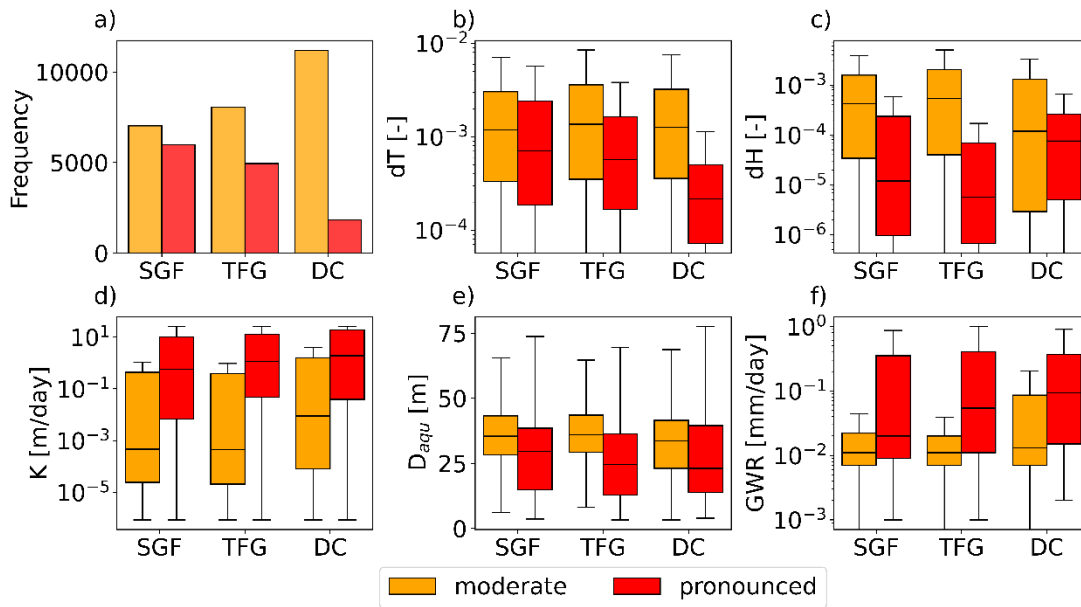


255  
 256 **Figure 2** – Boxplots of a) topographic gradient (dT), b) hydraulic gradient (dH), c) hydraulic  
 257 conductivity (K), d) aquifer depth ( $D_{aqu}$ ), and e) groundwater recharge (GWR) in coastline cells  
 258 (i.e., cells with one side facing an ocean) without saline groundwater (blue), coastline cells with  
 259 saline groundwater (orange), and inland cells with saline groundwater (red). Subplots a), b), c) and  
 260 e) are in logarithmic scale and hence do not show 0 on the y-axis (see Fig S5 for plot without  
 261 logarithmic scales).

262 **3.2 Several factors control coastal groundwater salinity at the continental scale**

263 We apply thresholds (Table 1) to categorize saline groundwater fraction (SGF), the thickness of  
 264 fresh groundwater (TFG) column, and the distance of saline groundwater from the coast (DC) into  
 265 moderate and pronounced to assess which parameters control the severity of an aspect of coastal  
 266 saline groundwater in a cell. Pronounced salinization appears in 14-46% of saline cells (Fig 3 a)).  
 267 Lower topographic gradients (dT) allow saline groundwater to intrude farther from the coast (DC)  
 268 (Fig 3 b)). Cells with lower hydraulic gradients (dH) are more often exposed to higher saline  
 269 groundwater fractions (SGF) and lower thicknesses of fresh groundwater columns (TFG) (Fig 3  
 270 c)). Higher hydraulic conductivity (K) increases the exposure to all three aspects of saline  
 271 groundwater, illustrated by the approximately two orders of magnitude between the median  
 272 hydraulic conductivity (K) in cells with moderate and pronounced aspects (Fig 3 d)). The  
 273 distributions of aquifer depth ( $D_{aqu}$ ) in cells with moderate and pronounced aspects of saline  
 274 groundwater are similar (Fig 3 e)). Groundwater recharge (GWR) values are higher in cells with  
 275 pronounced aspects of saline groundwater (Fig 3 f)). The usage of thresholds other than

276 those described in Table 1 leads to similar results (Fig S6 and Fig S7), and a scatterplot version of  
 277 Figure 3 can be found in Figure S8.



278  
 279 **Figure 3** – Subplot a) shows the number of cells with moderate (orange) and pronounced (red)  
 280 Saline Groundwater Fraction (SGF), Thickness of Fresh Groundwater (TFG), and Distance of  
 281 saline groundwater from Coast (DC). Aspects of saline groundwater in cells are categorized as  
 282 pronounced if  $SGF > 0.5$ ,  $TFG < 5$  m, and  $DC > 10$  km. The remaining subplots show boxplots of  
 283 cells with moderate and pronounced SGF, TFG, and DC for b) topographic gradient (dT), c)  
 284 hydraulic gradient (dH), d) hydraulic conductivity (K), e) aquifer depth ( $D_{aqu}$ ), and f) groundwater  
 285 recharge (GWR).

#### 286 4 Discussion

287 Simulating the North American groundwater salinity distribution, we find results that align with  
 288 the literature, identifying aquifers with lower topographic gradient to the coast (Michael et al.,  
 289 2013), lower hydraulic gradient (Ferguson and Gleeson, 2012), and larger aquifer thickness (Mazi  
 290 et al., 2013) as more vulnerable towards containing saline groundwater at shallower depth and  
 291 further from the coast. Figure 3 suggests that while saline groundwater can be expected in regions  
 292 with hydraulic gradients below  $10^{-3}$ , which has been used by Ferguson and Gleeson (2012), high  
 293 exposure to saline groundwater can be expected at hydraulic gradients below  $10^{-4}$ . Of the North  
 294 American coastline cells classified by Michael et al. (2013) as topography-limited and thus

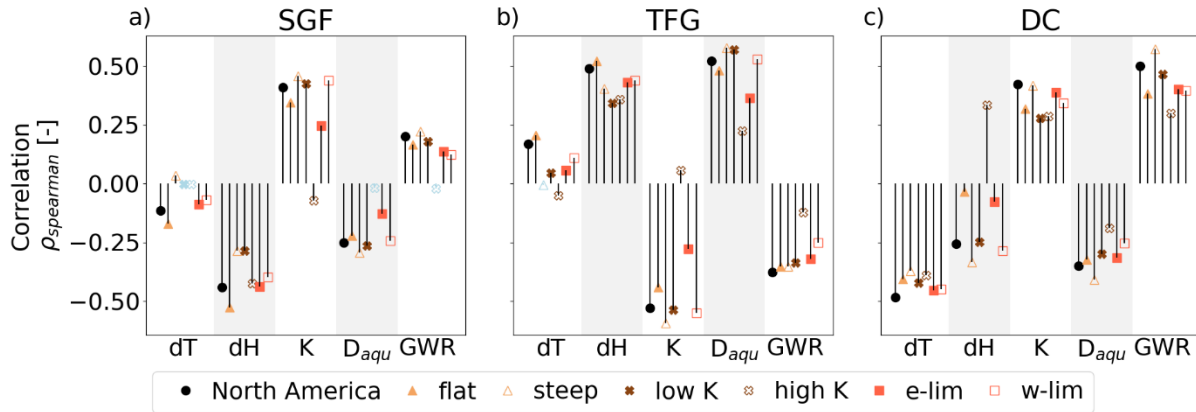
295 particularly vulnerable to seawater intrusion from sea level rise, 63% contain saline water in the  
296 presented simulation. In comparison, only 47% of cells in recharge-limited regions contain saline  
297 groundwater, which indicates that topography-limited cells may already (i.e., without sea level rise)  
298 be more likely to contain saline groundwater due to their relatively flat topography.

299 Our results show that inland cells with hydraulic conductivity ( $K$ ) above  $10^{-2}$  m day<sup>-1</sup> are  
300 particularly vulnerable to containing saline groundwater. This is consistent with our understanding  
301 that saline groundwater can be found where hydraulic conductivity is high enough for substantial  
302 groundwater flows (e.g., Shi and Jiao, 2014; Deng et al., 2017; Costall et al., 2020). However, the  
303 model does not contain conduits (e.g., in karstic or volcanic aquifers) or related focused  
304 groundwater exchanges between aquifers and the ocean (Kreyns et al., 2020), limiting its  
305 applicability in regions with such lithology. Surprisingly, groundwater recharge (GWR) values are  
306 higher in cells with pronounced aspects of saline groundwater (Fig 3 f)), indicating that more saline  
307 water spreads into regions with higher groundwater recharge. Such behavior has been reported for  
308 groundwater recharge below 100 mm yr<sup>-1</sup> (Michael et al., 2013). In cells with groundwater recharge  
309 above 100 mm yr<sup>-1</sup>, resilience against saline groundwater (i.e., SGF, TFG and DC) increases with  
310 increasing groundwater recharge (GWR) (Fig S9). However, the influence of groundwater recharge  
311 on the aspects of saline groundwater is low, potentially because topography is the main control in  
312 the applied groundwater model (Reinecke et al., 2024).

313 Across the North American continent, we identify coastal saline groundwater, in particular in  
314 Florida (US), along the US East Coast, and in Mexico (Fig S3), where issues with SWI have been  
315 reported (Barlow and Reichard, 2010). Additionally, we identified regions prone to containing  
316 saline groundwater, which have hardly been studied, in Alaska (US), Nunavut (Canada), and  
317 Oaxaca (Mexico). Using simple assumptions to estimate the vulnerability towards containing saline  
318 water (see Text S3), find that 23%/49% of the coastal area could be vulnerable due to low  
319 hydraulic/topographic gradients, while 68% of the coastal area could be vulnerable due to high  
320 hydraulic conductivities. However, parameter interactions limit the simulated area with saline  
321 groundwater to 18.6% (520 122 km<sup>2</sup>) of the coastal zone.

322 Although the influence of factors on the distribution of saline groundwater is evident, it does not  
323 show the full picture. Computing Spearman rank correlations of the factors with aspects of saline  
324 groundwater shows that weak to moderate monotonic relationships exist between most factors and  
325 aspects of saline groundwater (Fig 4). Scatter plots indicate non-monotonic relationships of factor

326 values with aspects of groundwater salinity (see Fig S8, Fig S10-S12), likely caused by factor  
 327 interactions not captured by Spearman rank correlations. Text S2 provides a detailed description of  
 328 Figure 4.



329  
 330 **Figure 4** – Spearman rank correlation of a) Saline Groundwater Fraction (SGF), b) Thickness of  
 331 Fresh Groundwater column (TFG), c) Distance of saline groundwater from coast (DC) with  
 332 topographic gradient (dT), hydraulic gradient (dH), hydraulic conductivity (K), aquifer depth  
 333 ( $D_{aqu}$ ) and groundwater recharge (GWR). Thresholds for the delineation of flat/steep, low/high K,  
 334 energy-/water-limited (e-/w-lim) regions are given in Table S2. Insignificant correlations are  
 335 shown in light blue. All correlations and p-values are displayed in Tables S4 to S6.

336 For saline water transport, the model’s spatial resolution of 5 arcmin is very coarse. Due to the  
 337 horizontal sharp interfaces applied, saline water entering a model cell on one side may cause the  
 338 horizontal interface to lift up. This shift in interface height entails that the saline water entering at  
 339 one time step may be transferred further to another neighboring cell in the next simulation step,  
 340 enabling saline water transport of several kilometers in just a year. Thus, the applied model likely  
 341 overestimates saline groundwater movement compared to real-world dispersive transfer. Despite  
 342 the likely faster movement of the saline interface, the model required 492 000 years to reach a state  
 343 of very slow interface movement, indicating that the saline groundwater distribution in North  
 344 America has been evolving since before the end of the last ice age, approximately 20 000 years  
 345 ago.

## 346 5 Conclusions

347 Given rapidly evolving coastal communities and growing demand for fresh groundwater in large  
 348 parts of North America, improving our understanding of continental coastal groundwater salinity

349 is pivotal. To assess the dominant controls of coastal saline groundwater occurrence and incursion  
350 at the continental scale, we have simulated variable density groundwater flow in North America  
351 until the sharp interface between fresh and saline water was stable under steady climatic forcing.  
352 Assessing the parameter values of fresh and saline cells at the coastline, we find that low  
353 topographic gradients and high aquifer depths enable saltwater to enter coastal aquifers. We show  
354 that coastline and inland cells are more vulnerable to containing saline groundwater if topographic  
355 gradients are lower and hydraulic conductivities are higher. Focusing on three aspects of coastal  
356 groundwater salinity, we show that under steady inputs, hydraulic gradient, topographic gradient,  
357 hydraulic conductivity, and aquifer depth control the salinity of coastal and inland cells. The impact  
358 of groundwater recharge seems to be limited in G<sup>3</sup>M-D. Our model results align with previous  
359 results identifying hydraulic conductivity as control in saline groundwater distribution. With  
360 hydraulic conductivities over  $10^{-2}$  m day<sup>-1</sup>, 68% of the North American coastal zone (i.e., up to 100  
361 km onshore and up to 100 m elevation) is, in principle, likely to carry saline groundwater. However,  
362 parameter interactions limit the simulated area with saline water to 18.6% of the North American  
363 coastal zone. Future research should assess the parameter interactions and use transient simulations  
364 to examine how changes in groundwater recharge and sea level rise impact seawater intrusion,  
365 particularly in regions with high hydraulic conductivities and low elevation.

## 366 **Data and Code availability**

- 367 • The code of G<sup>3</sup>M and G<sup>3</sup>M-D is available at: [https://github.com/rreinecke/global-gradient-](https://github.com/rreinecke/global-gradient-based-groundwater-model)  
368 [based-groundwater-model](https://github.com/rreinecke/global-gradient-based-groundwater-model)
- 369 • The North America model of G<sup>3</sup>M-D is available at:  
370 <https://github.com/EarthSystemModelling/3GM-D-NorthAmerica> (includes the code of  
371 G<sup>3</sup>M-D as a git submodule)
- 372 • The elevation data by Lehner et al. (2008) is available at:  
373 <https://www.hydrosheds.org/products/hydrosheds>
- 374 • The groundwater recharge data by Müller Schmied et al. (2020) is available at:  
375 <https://doi.pangaea.de/10.1594/PANGAEA.918447>
- 376 • The GLHYMPS 2.0 data (including hydraulic conductivity and effective porosity) by  
377 Huscroft et al. (2018) is available at:  
378 <https://borealisdata.ca/dataset.xhtml?persistentId=doi%3A10.5683/SP2/TTJNIU>



- 379 • The CoPerm data (used to set the hydraulic conductivity of the general head boundary) by  
380 Moosdorf et al. (2024) is available at: <https://doi.pangaea.de/10.1594/PANGAEA.958901>
- 381 • The depth to bedrock data (used to set aquifer depth) by Shangguan et al. (2017) is available  
382 at: <http://globalchange.bnu.edu.cn/research/dtb.jsp>
- 383 • The groundwater heads and interface heights of the final time step, which are evaluated in  
384 this study, are available at: [10.5281/zenodo.13928185](https://zenodo.org/record/13928185)

385

### 386 **Funding statement / Acknowledgements**

387 DK is funded by Deutsche Forschungsgemeinschaft (GZ: RE 4624/1-1). RR and TW were funded  
388 by the Alexander von Humboldt Foundation in the framework of the Alexander von Humboldt  
389 Professorship endowed by the German Federal Ministry of Education and Research. HM was  
390 funded by the US National Science Foundation Coastal Critical Zone project (EAR2012484). MB  
391 was funded by the ERC Advanced Grant Scheme (project GEOWAT no. 101019185). NM  
392 Acknowledges funding from DFG MO 2538/8-1.

393 **Conflicts of interest:** None

### 394 **References**

- 395 Bakker M, Schaars F, Hughes J D, Langevin C D, and Dausman A M 2013 Documentation of the  
396 Seawater Intrusion (SWI2) Package for MODFLOW: U.S. Geological Survey Techniques and  
397 Methods, book 6, chap. A46, 47 p. <https://pubs.usgs.gov/tm/6a46/>
- 398 Barlow P M and Reichard E G 2010 Saltwater intrusion in coastal regions of North America  
399 *Hydrogeol. J.* **18**(1):247–260 doi: [10.1007/s10040-009-0514-3](https://doi.org/10.1007/s10040-009-0514-3)
- 400 Befus K M, Barnard P L, Hoover D J, Finzi Hart J A, and Voss C I 2020 Increasing threat of coastal  
401 groundwater hazards from sea-level rise in California *Nature Climate Change* **10**(10):946–952 doi:  
402 [10.1038/s41558-020-0874-1](https://doi.org/10.1038/s41558-020-0874-1)
- 403 Cao T, D Han, and X Song 2021 Past, present, and future of global seawater intrusion research: A  
404 bibliometric analysis *Journal of Hydrology* **603**:126844 doi: [10.1016/j.jhydrol.2021.126844](https://doi.org/10.1016/j.jhydrol.2021.126844)

405 Costall A R, Harris B D, Teo B, Schaa R, Wagner F M, and Pigois J P 2020 Groundwater  
406 throughflow and seawater intrusion in high quality coastal aquifers *Scientific Reports* **10**(1): 9866  
407 doi: 10.1038/s41598-020-66516-6

408 Custodio E 2010 Coastal aquifers of Europe: an overview *Hydrogeol. J.* **18**(1):269–280 doi:  
409 10.1007/s10040-009-0496-1

410 Deng Y, Young C, Fu X, Song J, and Peng Z-R 2017 The integrated impacts of human activities  
411 and rising sea level on the saltwater intrusion in the east coast of the Yucatan Peninsula, Mexico  
412 *Nat. Hazards* **85**(2): 1063–1088 doi: 10.1007/s11069-016-2621-5

413 Dieter C A, Linsey K S, Caldwell R R, Harris M A, Ivahnenko T I, Lovelace J K, Maupin M A,  
414 and Barber N L 2018 Estimated Use of Water in the United States County-Level Data for 2015  
415 (ver. 2.0, June 2018): U.S. Geological Survey data release doi: 10.5066/F7TB15V5

416 Feth J H 1965 Preliminary Map of the Conterminous United States Showing Depth to and Quality  
417 of Shallowest Ground Water Containing More Than 1,000 Parts Per Million Dissolved Solids:  
418 Hydrologic Investigations Atlas HA-199, 31 p.

419 Gnann S, et al. 2023 Functional relationships reveal differences in the water cycle representation  
420 of global water models *Nat. Water* **1**:1079–1090 doi: 10.1038/s44221-023-00160-y

421 Harbaugh A W 2005 MODFLOW-2005, the U.S. Geological Survey modular groundwater model  
422 – the Ground-Water Flow Process. *U.S. Geological Survey Techniques and Methods* 6-A16

423 Henry H R 1964 Effect of Dispersion on Salt Encroachment in Coastal Aquifers. U.S. Geological  
424 Survey Water-Supply, Paper 1613-C, 70-84

425 Huscroft J, Gleeson T, Hartmann J, and Börker J 2018 Compiling and Mapping Global  
426 Permeability of the Unconsolidated and Consolidated Earth: GLobal HYdrogeology MaPS 2.0  
427 (GLHYMPS 2.0) *Geophys. Res. Lett.* **45**(4):1897–1904. doi: 10.1002/2017GL075860

428 Jasechko S, Perrone D, and Seybold H 2020 Groundwater level observations in 250,000 coastal  
429 US wells reveal scope of potential seawater intrusion *Nature communications* **11**(1): 3229 doi:  
430 10.1038/s41467-020-17038-2

431 Ketabchi H, Mahmoodzadeh D, Ataie-Ashtiani B, and Simmons C T 2016 Sea-level rise impacts  
432 on seawater intrusion in coastal aquifers: Review and integration *Journal of Hydrology* **535**:235-  
433 255 doi: 10.1016/j.jhydrol.2016.01.083

434 Lehner B, Verdin K, and Jarvis A 2008 New global hydrography derived from spaceborne  
435 elevation data *Eos, Transactions American Geophysical Union* **89**(10):93–94 doi:  
436 10.1029/2008EO100001

437 Manivannan V and Elango L 2019 Seawater intrusion and submarine groundwater discharge along  
438 the Indian coast *Environmental science and pollution research* **26**(31):31592–31608 doi:  
439 10.1007/s11356-019-06103-z

440 Michael H A, Russoniello C J, and Byron L A 2013 Global assessment of vulnerability to sea-level  
441 rise in topography-limited and recharge-limited coastal groundwater systems *Water Resources*  
442 *Research* **49**(4):2228–2240 doi: 10.1002/wrcr.20213

443 Moosdorf N, Tschaikowski J, Kretschmer D, and Reinecke R 2024 A global coastal permeability  
444 dataset (CoPerm 1.0) *Scientific Data* **11**(1):893, 2024 doi: 10.1038/s41597-024-03749-4

445 Müller Schmied H et al. 2020 The global water resources and use model WaterGAP v2.2d -  
446 Standard model output [dataset] *PANGAEA* doi: 10.1594/PANGAEA.918447

447 Neumann B, Vafeidis A T, Zimmermann J, and Nicholls R J 2015 Future coastal population growth  
448 and exposure to sea-level rise and coastal flooding—a global assessment *PloS one* **10**(3):e0118571  
449 doi:10.1371/journal.pone.0118571

450 Post V E A, Eichholz M, and Brentführer R 2018 Groundwater management in coastal zones.  
451 Bundesanstalt für Geowissenschaften und Rohstoffe (BGR). Hannover, Germany, 107 pp.

452 Reilly T E, Dennehy K F, Alley W M, and Cunningham W L 2008. Ground-Water Availability in  
453 the United States: U.S. Geological Survey Circular 1323, 70 p.

454 Reinecke R, Foglia L, Mehl S, Herman J D, Wachholz A, Trautmann T, and Döll P 2019a Spatially  
455 distributed sensitivity of simulated global groundwater heads and flows to hydraulic conductivity,  
456 groundwater recharge, and surface water body parameterization *Hydrology and Earth System*  
457 *Sciences* **23**(11):4561–4582 doi: 10.5194/hess-23-4561-2019

458 Reinecke R, Foglia L, Mehl S, Trautmann T, Cáceres D, and Döll P 2019 Challenges in developing  
459 a global gradient-based groundwater model (G<sup>3</sup>M v1.0) for the integration into a global  
460 hydrological model *Geoscientific Model Development* **12**(6):2401–2418 doi: 10.5194/gmd-12-  
461 2401-2019

462 Reinecke R et al. 2024 Uncertainty in model estimates of global groundwater depth. *Environmental*  
463 *Research Letters*, [in press] doi: 10.1088/1748-9326/ad8587

464 Richardson C M, Davis K L, Ruiz-González C, Guimond J A, Michael H A, Paldor A, Moosdorf  
465 N and Paytan A 2024 The impacts of climate change on coastal groundwater *Nature Reviews Earth*  
466 *& Environment* **5**:100–119 doi: 10.1038/s43017-023-00500-2

467 Sawyer A H, David C H, and Famiglietti J S 2016 Continental patterns of submarine groundwater  
468 discharge reveal coastal vulnerabilities *Science* **353**(6300):705-707 doi: 10.1126/science.aag1058

469 Shangguan W, Hengl T, Mendes J J, Yuan H, and Dai Y 2017 Mapping the global depth to bedrock  
470 for land surface modeling *Journal of Advances in Modeling Earth Systems* **9**(1): 65-88 doi:  
471 10.1002/2016MS000686

472 Shi L and Jiao J J 2014 Seawater intrusion and coastal aquifer management in China: a review  
473 *Environmental Earth Sciences* **72**(8):2811–2819 doi: 10.1007/s12665-014-3186-9

474 Weedon G P, Balsamo G, Bellouin N, Gomes S, Best M J, and Viterbo P 2014 The WFDEI  
475 meteorological forcing data set: WATCH Forcing Data methodology applied to ERA-Interim  
476 reanalysis data *Water Resources Research* **50**:7505–7514 doi: 10.1002/2014WR015638

477 Werner A D and Simmons C T 2009 Impact of sea-level rise on sea water intrusion in coastal  
478 aquifers *Ground Water* **47**(2):197–204 doi: 10.1111/j.1745-6584.2008.00535.x

479 Wilson S and Fischetti T 2010 Coastline population trends in the United States: 1960 to 2008:  
480 Population estimates and projections. U.S. Census Bureau.

481 Zamrsky D, Oude Essink G H P, and Bierkens M F P 2024 Global impact of sea level rise on  
482 coastal fresh groundwater resources *Earth's Future* **12**(1) doi: 10.1029/2023EF003581